A Hybrid Material Approach Toward Solution-Processable Dielectrics Exhibiting Enhanced Breakdown Strength and High Energy Density

*Kuo Han, Qi Li, Chalathorn Chanthad, Matthew R. Gadinski, Guangzu Zhang, and Qing Wang**

The ever-increasing demand for compact electronics and electrical power systems cannot be met with conventional dielectric materials with limited energy densities. Numerous efforts have been made to improve the energy densities of dielectrics by incorporating ceramic additives into polymer matrix. In spite of increased permittivities, thus-fabricated polymer nanocomposites typically suffer from significantly decreased breakdown strengths, which preclude a substantial gain in energy density. Herein, organic–inorganic hybrids as a new class of dielectric materials are described, which are prepared from the covalent incorporation of tantalum species into ferroelectric polymers via in situ sol-gel condensation. The solution-processed hybrid with the optimal composition exhibits a Weibull breakdown strength of 505 MV m^{-1} and a discharged energy density of 18 J cm^{-3}, which are more than 40% and 180%, respectively, greater than the pristine ferroelectric polymer. The superior performance is mainly ascribed to the deep traps created in the hybrids at the molecular level, which results in reduced electric conduction and lower remnant polarization. Simultaneously, the formation of the cross-linked networks enhances the mechanical strengths of the hybrid films and thus hinders the occurrence of the electromechanical breakdown. This work opens up new opportunities to solution-processed organic materials with high energy densities for capacitive electrical energy storage.

1. Introduction

The substitution of intermittent renewable energy sources such as wind and solar for fossil fuels would be propelled by the development of energy storage technologies that are able to balance the supply and demand of energy.[1,2] However, the performance of current energy storage devices falls well short of future energy needs. For instance, the next generation of hybrid and electric vehicles calls for compact and low-cost energy storage devices with substantially high energy and power densities and great charge–discharge cyclability. Compared to the electrochemical devices such as batteries and fuel cells, dielectric capacitors possess higher power density, faster charge–discharge capability, and longer lifetime,[3,4] but bear energy densities that are one order of magnitude lower than those of batteries.[5] As the energy density of capacitors is governed by the dielectric materials that separate the opposite static charges between two electrodes, the development of dielectric materials with greatly improved energy density is thus becoming one of the major enabling technologies.[6]

In general, the energy density (U_e) of linear dielectric materials is given by $U_e = ½ \varepsilon_r\varepsilon_0 E^2$, where ε_r is the effective permittivity, ε_0 is the vacuum permittivity, and E is the applied field. Inorganic dielectric materials, while enjoying high dielectric permittivities, are limited by low breakdown strength (E_b), i.e., typically in the scale of kV m^{-1}. On the other hand, polymer dielectrics possess excellent processability, low cost, light weight, high E_b (in the scale of MV m^{-1}), and graceful failure mechanism, although their permittivities are orders of magnitude smaller than those of their inorganic counterparts.[7,8] To integrate the complementary advantages of inorganic and organic dielectric materials, polymer nanocomposites composed of inorganic ceramic fillers with high dielectric constant (k) have been prepared by using a variety of methods, including mechanical blending,[9,10] solution mixing,[11–15] and surface-initiated polymerization.[16,17] As expected, k values of the polymer nanocomposites have indeed been improved, but there exist serious drawbacks in the nanocomposite approach. (1) The presence of a large contrast in k values between two phases augments the local electric field distortions and results in a highly inhomogeneous field distribution, and consequently, decreases E_b.[4] As U_e of dielectrics scales as the second power of the applied electric field, a reduced E_b would diminish any substantial improvement in energy storage capability even though k is increased. (2) The structural imperfections at the filler/matrix interface such as flaws and voids caused by the poor filler distribution and incompatibility between the inorganic and organic phases not only are detrimental to E_b, but also give rise to large conduction loss. This, in turn, reduces the discharged energy density and shortens the lifetime of devices because of Joule heating.

Dr. K. Han, Dr. Q. Li, Dr. C. Chanthad, M. R. Gadinski, Dr. G. Zhang, Prof. Q. Wang
Department of Materials Science and Engineering
The Pennsylvania State University
University Park, PA 16802, USA
E-mail: wang@matse.psu.edu

DOI: 10.1002/adfm.201501070

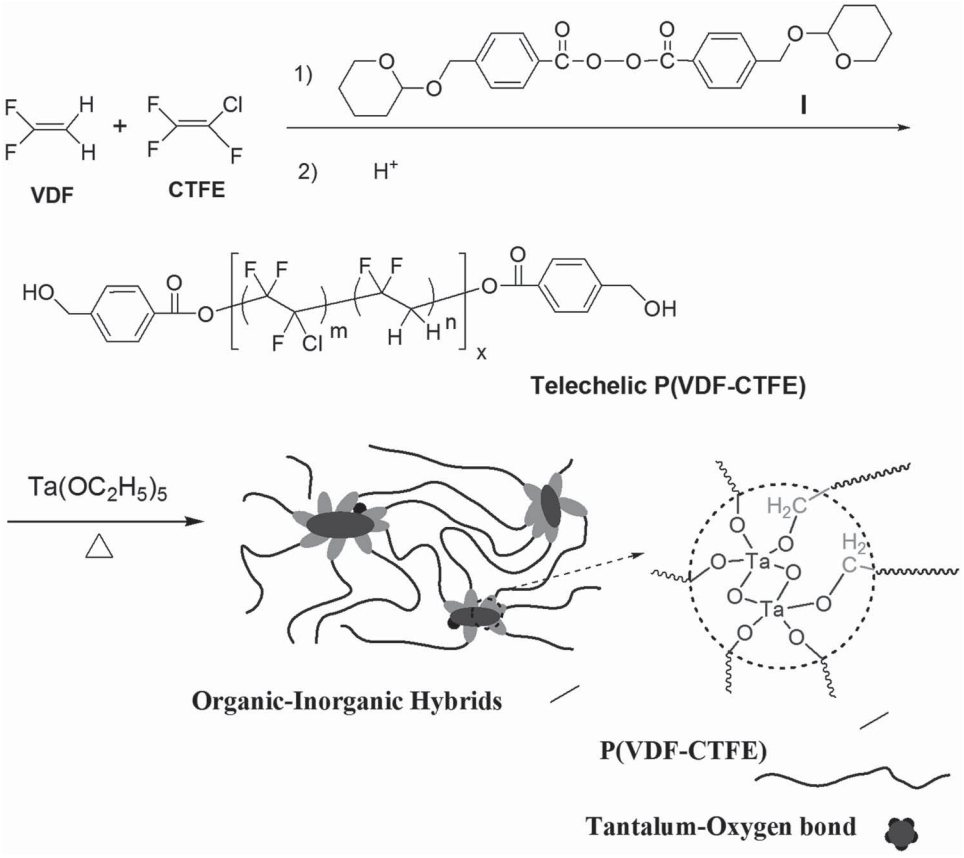

Figure 1. Synthesis of the organic–inorganic hybrids from sol-gel condensation of chain-end functionalized P(VDF-CTFE).

Although chemical modifications of the surface of inorganic fillers have proven effective in improving interfacial compatibility,[18,19] the tethered ligand with long hydrocarbon chains is highly vulnerable under high fields due to its low dielectric permittivity.[20] Therefore, the potential gain in U_e by means of simply mixing high-k inorganic fillers with polymer dielectrics is rather limited.

Among various dielectric polymers, ferroelectric polymers represented by poly(vinylidene fluoride) (PVDF) and its co- and ter-polymers possess the highest k and state-of-the-art U_e as a result of high polarization arising from the C—F bonds and spontaneous orientation of the dipoles in the crystalline domains.[21–24] As E_b plays a vital role in determining U_e, several strategies have been carried out to improve E_b of ferroelectric polymers. Mechanical stretching-based processing techniques have shown to be very efficient in enhancing the dielectric strength of PVDF-based ferroelectric polymers by improving mechanical strength and reducing ionic conduction of films.[8,11,25] However, stretching simultaneously converts the chain conformation of PVDF to all-*trans* and induces the formation of β-phase crystalline structures, which unfortunately leads to pronounced hysteresis loss and degrades the discharged energy density.[26] For ferroelectric polymer nanocomposites, 1D nanostructures such as TiO_2 and $BaTiO_3$ nanowires[27,28] and 2D nanoplates such as boron nitride nanosheets[29,30] have been successfully introduced into the polymer matrix. The enhanced E_b of the polymer nanocomposites have been credited to the optimization of local field distribution, the addition of scattering centers, and the creation of barriers in the electrical tree growth during breakdown.[31,32]

In this contribution, we report high-performance solution-processed dielectric materials derived from sol-gel condensation of tantalum alkoxide and hydroxyl-terminated ferroelectric polymer. Different from the conventional dielectric nanocomposites based on nano or micro-sized fillers, the organic–inorganic hybrids contain inorganic units that are covalently incorporated into the ferroelectric polymers at the molecular scale. It is found that the hybrids exhibit many ideal features for high-field capacitive energy storage, including lower dielectric loss, superior breakdown strength and greater dielectric reliability, and higher discharged energy density with respect to the neat ferroelectric polymer.

2. Results and Discussion

2.1. Synthesis and Structure Characterization

Ferroelectric poly(vinylidene fluoride-*co*-chlorotrifluoroethylene), P(VDF-CTFE), is chosen as the matrix in this work, which is modified with tantalum–oxygen (Ta–O) segments. Tantalum pentoxide (Ta_2O_5) has received considerable attention recently as a new generation of dielectrics to substitute SiO_2 in microelectronic devices because of its high dielectric constant (e.g., >20 depending on deposition conditions), and chemical and thermal stability.[33,34] **Figure 1** illustrates the synthetic

route to the organic–inorganic hybrids, which includes the preparation of the telechelic P(VDF-CTFE) with hydroxyl terminal groups and subsequent sol-gel condensation with tantalum ethoxide ($Ta(OCH_2CH_3)_5$).

Telechelic P(VDF-CTFE) was synthesized via free radical polymerization of VDF and CTFE using 4-[(tetrahydropyran-2-yloxy) methyl] benzoic peroxide (**I**) as the initiator.[35] The initiator **I** was afforded by the coupling of the benzoic acid in the presence of H_2O_2 and *N,N′* dicyclohexylcarbodiimide (DCC) (see the Supporting Information, Figure S1). Since the termination in radical polymerization of fluorinated alkenes proceeds predominately through the radical coupling reaction, the tetrahydropyran (THP)-protected hydroxyl groups in the initiator **I** were successfully transferred to the polymer chain ends after polymerization. The ^{1}H NMR spectrum of the chain-end functionalized P(VDF-CTFE) after deprotection (Supporting Information, Figure S2) clearly shows the signals at 4.63, 7.61, and 7.98 ppm corresponding to the protons from benzylic and phenyl groups, respectively, indicative of the presence of benzylic groups at the polymer chain ends. The prepared P(VDF-CTFE) was determined to contain 90 mol% VDF and 10 mol% CTFE according to the integrals of the characteristic peaks of VDF and CTFE in the ^{19}F NMR spectrum (Supporting Information, Figure S2). End-group analysis based on the ^{1}H and ^{19}F NMR spectra revealed a number-average molecular weight (M_n) of 45 000 g mol^{-1} of the chain-end functionalized P(VDF-CTFE), while triple-detection gel permeation chromatography (GPC) measurements in DMF gave an M_n of 43 000 g mol^{-1} and a polydispersity of ~1.4. The average degree of functionality was calculated to about 1.9, near the expected theoretical values of 2.

The hybrids were prepared from the acid-catalyzed sol-gel reaction between the telechelic P(VDF-CTFE) ended with benzyl alcohols and $Ta(OCH_2CH_3)_5$ with varied ratios under heating. The hybrids prepared from 5, 9, 13, 17, and 23 wt% $Ta(OCH_2CH_3)_5$ are referred to as **H1–5**, respectively. The condensation was confirmed by the appearance of new absorbance at around 600 cm^{-1} attributed to Ta—O—Ta stretching whose relative intensity increases steadily with the increase of the loading of $Ta(OCH_2CH_3)_5$ in the FTIR spectra of the hybrids (**Figure 2**).[36–38] The formation of the cross-linking networks upon the sol-gel condensation renders great thermal stability and improved mechanical properties of the hybrids. For example, the hybrids remain intact when heated at 200 °C overnight, whereas the telechelic P(VDF-CTFE) films melt at ~120 °C. Concurrently, the Young's modulus and tensile strength increase from 555 and 17 MPa of the telechelic P(VDF-CTFE) to 689 and 27 MPa of **H3**, and 827 and 28 MPa of **H5**, respectively. **Figure 3** shows the typical cross-sectional scanning electron microscopic (SEM) and transmission electron microscopic (TEM) images of the hybrid **H3**, which display homogeneous morphology and contain no discernible inorganic particle or agglomeration. By further increasing the Ta—O content, aggregation of the inorganic phase starts to emerge (Supporting Information, Figure S3) in the hybrids **H4** and **H5**.

Differential scanning calorimetry (DSC) and wide-angle X-ray diffraction (WAXD) measurements were carried out to examine the effect of the incorporated Ta-O segments on the microstructure of P(VDF-CTFE) matrix. As revealed in the DSC profile obtained in the cooling scan (Supporting Information, Figure S4), the crystallization temperature (T_c) is reduced gradually from 85 °C of the telechelic P(VDF-CTFE) to 67 °C of **H3**, which then increases to 74 °C of **H5** probably due to aggregation. Concomitantly, the enthalpy of melting decreases progressively from 29.5 J g^{-1} of P(VDF-CTFE) to 19.8 J g^{-1} of **H3** and 14.5 J g^{-1} of **H5**, respectively, which correspond to a change of the degree of crystallinity from 33.8% of the telechelic P(VDF-CTFE) to 24.5% of **H3** and 20.2% of **H5** (**Table 1**). The reduction of the degree of crystallinity, e.g., 34.2% of P(VDF-CTFE) to 26.2% of **H3**, upon the sol-gel reaction was also verified in WXAD measurements (Supporting Information, Figure S5). Furthermore, with increasing the Ta-O content, the major peak at a 2θ angle of 18° assigned to the (020) diffraction from the α phase becomes broader,[39] suggesting that the crystallite size is successively lowered from ~32 nm in the telechelic polymer to ~23 nm in **H3** and ~27 nm in **H5**. These trends are distinctively different from those found in conventional ferroelectric nanocomposites in which the nanosized ceramic particles function as nucleating agents to facilitate the crystallization of the polymer matrix, yielding constant increases in T_c.[40] On the contrary, it is believed that the incorporated Ta-O segments and the resultant cross-linked structures in the hybrids inhibit the crystallization of the ferroelectric polymer.

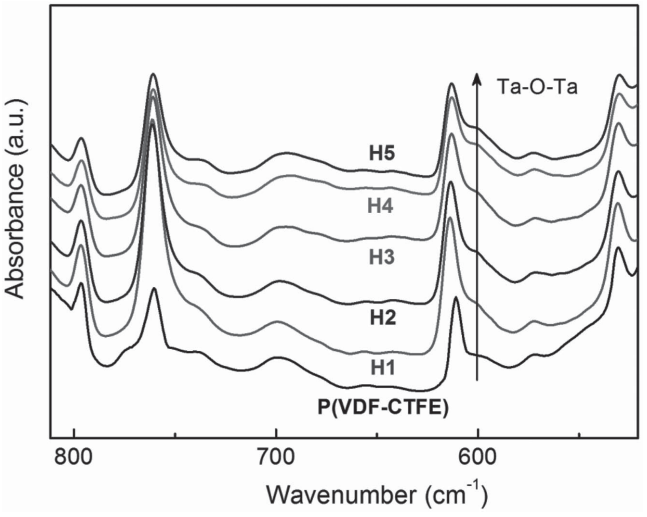

Figure 2. FTIR spectra of the telechelic P(VDF-CTFE) and the hybrids.

2.2. Dielectric Properties

Dielectric properties of the hybrids have been characterized as a function of frequency and temperature. As shown in **Figure 4**, compared to pristine P(VDF-CTFE) with a permittivity of 10.3 at 1 kHz, the prepared hybrids **H1–5** possess slightly decreased permittivities ranging from 10.1 to 9.7, owing to the confined chain motion and reduced dipole orientation as a result of cross-linking. In the meantime, the hybrids exhibit lower dielectric loss than the pristine polymers with the lowest value observed in **H3**, especially at low frequencies (i.e., < 100 kHz), which reaffirm the reduced chain mobility in the hybrids. The increase of loss tangents from **H3** to **H4** and **H5** can be traced to aggregation of the inorganic units at high contents.

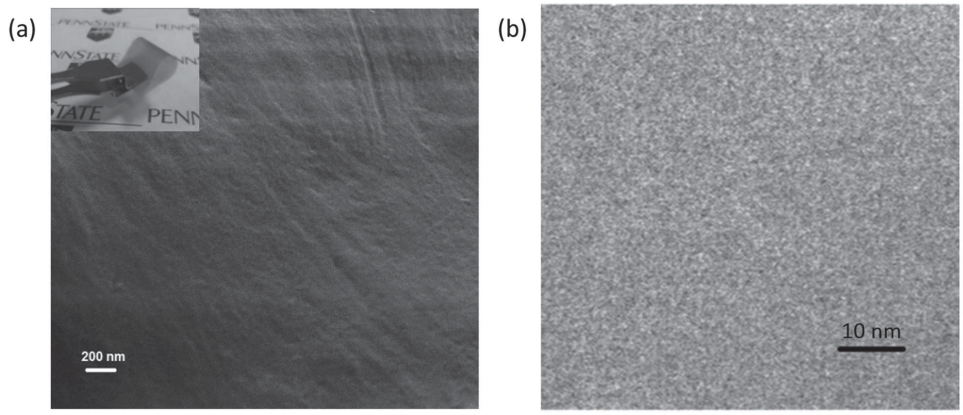

Figure 3. a) Cross-sectional SEM and b) TEM images of the hybrid **H3**. Inset (a), a photo of the prepared hybrid film. Scale bar, a) 200 nm, b) 10 nm.

The hybrids exhibit typical ferroelectric behavior with the dielectric peak shifting progressively to high temperature as frequency increases (**Figure 5**, Supporting Information, Figure S6), where the broad dielectric peaks are consequences of the kinetics associated with the dipolar glass freezing transition. A new dielectric peak centered at 24–26 °C shown in the spectra of the hybrids is assigned to the polymer chains bonded to Ta-O segments. The presence of this transition at higher temperature with respect to that of the pure polymer is apparently attributed to limited chain mobility caused by cross-linked structures in the hybrids, which increases the activation energy of the transition.[11] A major peak at about –28 °C in the loss spectra arises from the glass transition of the polymer. Moreover, compared to the neat polymer, the hybrids exhibit much lower dielectric loss at high temperatures, indicating that space charge conduction in the hybrids is significantly reduced. This is consistent with the dielectric and electrical conductivity results measured under high electric fields (see the sections below).

The representative loss spectra of the pristine polymer and hybrid **H3** at varied temperatures are compared in **Figure 6**, which is described well by the Arrhenius equation. The corresponding frequencies, f_{max}, versus the reciprocal temperature are plotted in the insets. By linear fitting the $\log(f_{max})$, the dielectric activation energies below and above the glass transition temperature (T_g) are calculated based on the Arrhenius equation and list in **Table 2**. The increase in the activation energy and energy barrier in the hybrids, e.g., 0.84 eV of **H3** versus 0.76 eV of P(VDF-CTFE), manifests retardation in dynamics of the polymer due to the formation of a cross-linked network and introduction of inorganic Ta-O linkages.

2.3. Electrical Conduction

While the hybrids show reduced dielectric loss at weak fields, as discussed in the section above, it is of importance to note that dielectric properties under high electric fields are very different from those shown in the dielectric spectra because of the field-dependent loss mechanism. Especially, electrical conduction, a general phenomenon to all dielectric materials, increases exponentially with the applied fields. To assess the high-field conduction loss, the current density of the hybrids was measured along with P(VDF-CTFE) under a field of 10 MV m^{-1} at 25 °C (**Figure 7**a). According to the equilibrium conductivity shown in Figure 7b, the hybrids all present much lower conductivities than the neat P(VDF-CTFE) and **H3** is found with the lowest electrical conductivity that is more than one order of magnitude smaller than that of P(VDF-CTFE). In concert with the trend shown in Figure 7b, the current density measured at various applied fields exhibits a strong dependence on the chemical compositions of the hybrids, where **H3** has the lowest current density (Figure 7c) among the dielectrics investigated in this study and the hybrids are much less conductive than P(VDF-CTFE). It is likely that the increase of the current density from **H3** to **H5** is again caused by the agglomeration of inorganic phase as observed in the TEM images (Supporting Information, Figure S3). The aggregates overlap the local conductive regions, leading to the increase of conduction and the decline of dielectric strength (see the discussions below).

The thermally stimulated discharge current (TSDC) measurements have been performed on the polymer and hybrids, where the samples are charged with a field of 10 MV m^{-1} at

Table 1. Crystallization parameters of the telechelic P(VDF-CTFE) and the hybrids.

	P(VDF-CTFE)	H1	H2	H3	H4	H5
Crystallinity [%] by DSC	33.8	30.2	25.0	24.5	23.1	20.2
Crystallinity [%] by XRD	34.2	31.7	26.7	26.2	25.1	21.5
Spacing *d* [Å] (from 020 peak)	4.81	4.84	4.85	4.83	4.86	4.85
Crystal size [nm] (from 020 peak)	32.2	28.9	27.6	23.4	25.5	26.8
T_m [°C]	113.6	113.0	109.5	106.7	110.8	111.5
T_c [°C]	83.0	78.7	74.5	67.4	73.4	74.8

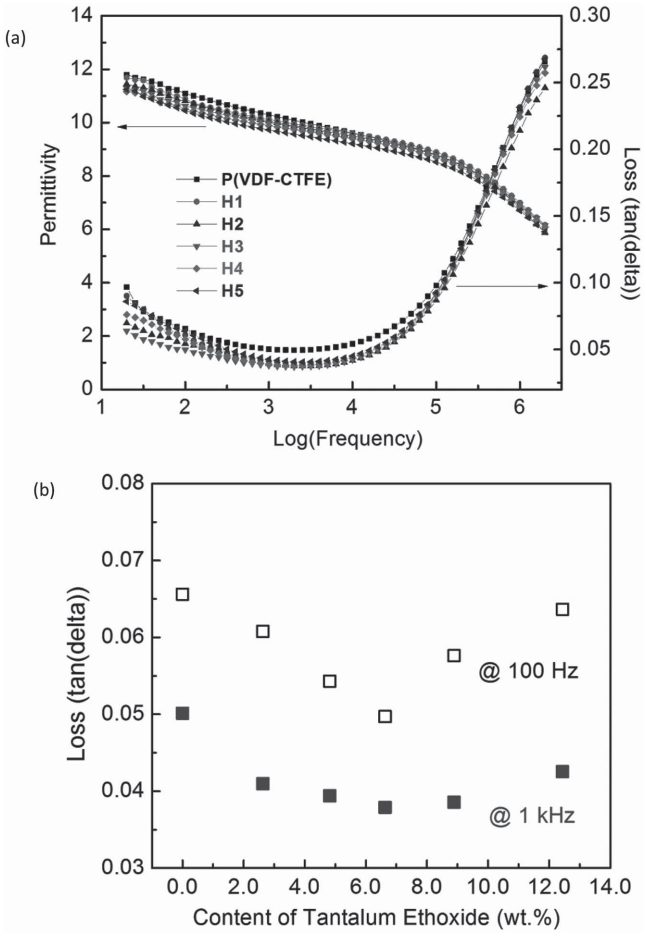

Figure 4. a) The permittivity and dielectric loss (tanδ) as a function of frequency at 25 °C for the telechelic P(VDF-CTFE) and the hybrids. b) Composition dependence of dielectric loss (tanδ) of the hybrids.

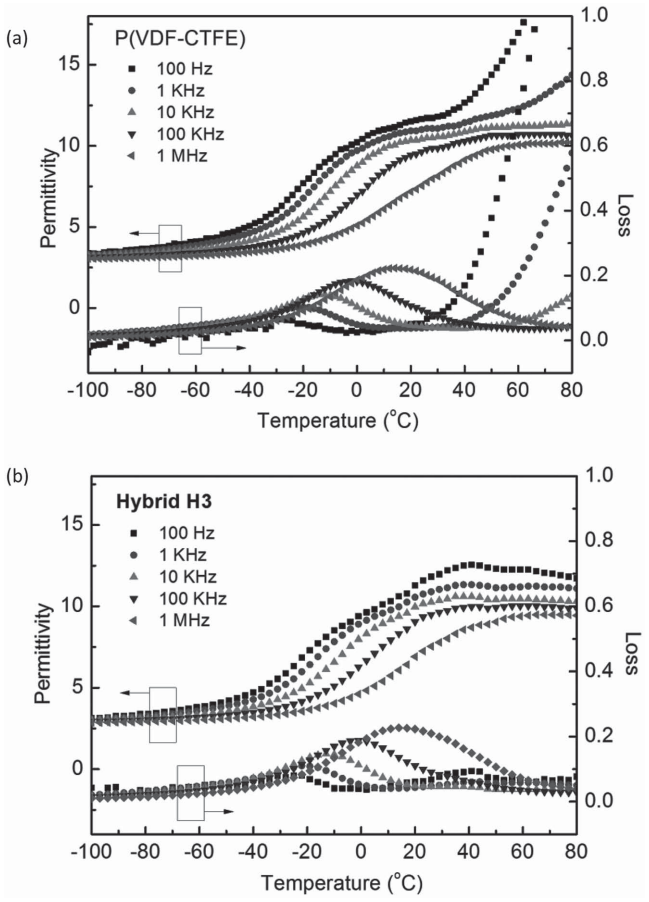

Figure 5. Temperature-dependent dielectric spectra of a) the telechelic P(VDF-CTFE) and b) the hybrid **H3**.

50 °C for 30 min and then rapidly cooled down to –100 °C with the applied electric field. Afterward, the electric field is removed and the samples are short circuited and heated to 100 °C at the rate of 5 °C min^{-1} with the current being measured across the samples. The TSDC curves of the pristine P(VDF-CTFE) and the hybrid **H3** are displayed in **Figure 8**. The β_a relaxation corresponds to the amorphous relaxation of the glass transition, whereas the β_c peak is ascribed to molecular motions in the crystalline region, which can be considered the depolarization process associated with ferroelectric–paraelectric phase transition of P(VDF-CTFE). The γ_L and γ_H peaks originate from the thermally activated space charge that is the major contribution to the high temperature dielectric loss.[41,42] It is evident that the peaks in **H3** shift to higher temperature as compared to those of the neat polymer. The shift of β_a and β_c relaxation indicates that cross-linking constrains the chain motion in both amorphous and crystalline phases. The upward shift of γ_L and appearance of a new high-temperature trap peak γ_H suggest the formation of deeper traps in the hybrids, which most likely stem from the cross-linking structures and Ta-O units. The TSDC results conclusively confirm that the reduced conduction loss of the hybrids in comparison to the neat polymer is attributable to the formation of deeper traps in the hybrid structures.

2.4. Dielectric Breakdown

Figure 9 compares the experimental characteristic E_b of P(VDF-CTFE) and the hybrids, whereas the breakdown results were analyzed using a two-parameter Weibull distribution function, $P = 1 - \exp(-(E_b/\alpha)\beta)$, where P is the cumulative probability of electric failure, α is the characteristic breakdown strength that corresponds to a ~63.2% probability of failure, and β is the slope parameter that evaluates the scatter of data. At least 15 measurements have been made for each Weibull fitting. The Weibull parameters of the hybrids are listed in **Table 3**. Compared to an E_b of 360 MV m^{-1} with a β of 7.45 for the solution-processed pristine P(VDF-CTFE), the hybrids display dramatically improved E_b and much higher β values, e.g., an E_b of 505 MV m^{-1} and a β of 15.29 are observed in **H3**, which denote its higher dielectric strength and reliability with respect to the neat polymer.

It is noteworthy that the composition dependence of dielectric strength in the hybrids agrees well with the trend shown in dependence of conductivity on the Ta-O content, further signifying the critical role of high-field conduction loss in dictating E_b. Additionally, it is commonly accepted that the electromechanical breakdown mechanism is responsible for electrical failure of ferroelectric polymers.[43] When a capacitor is charged, an attractive

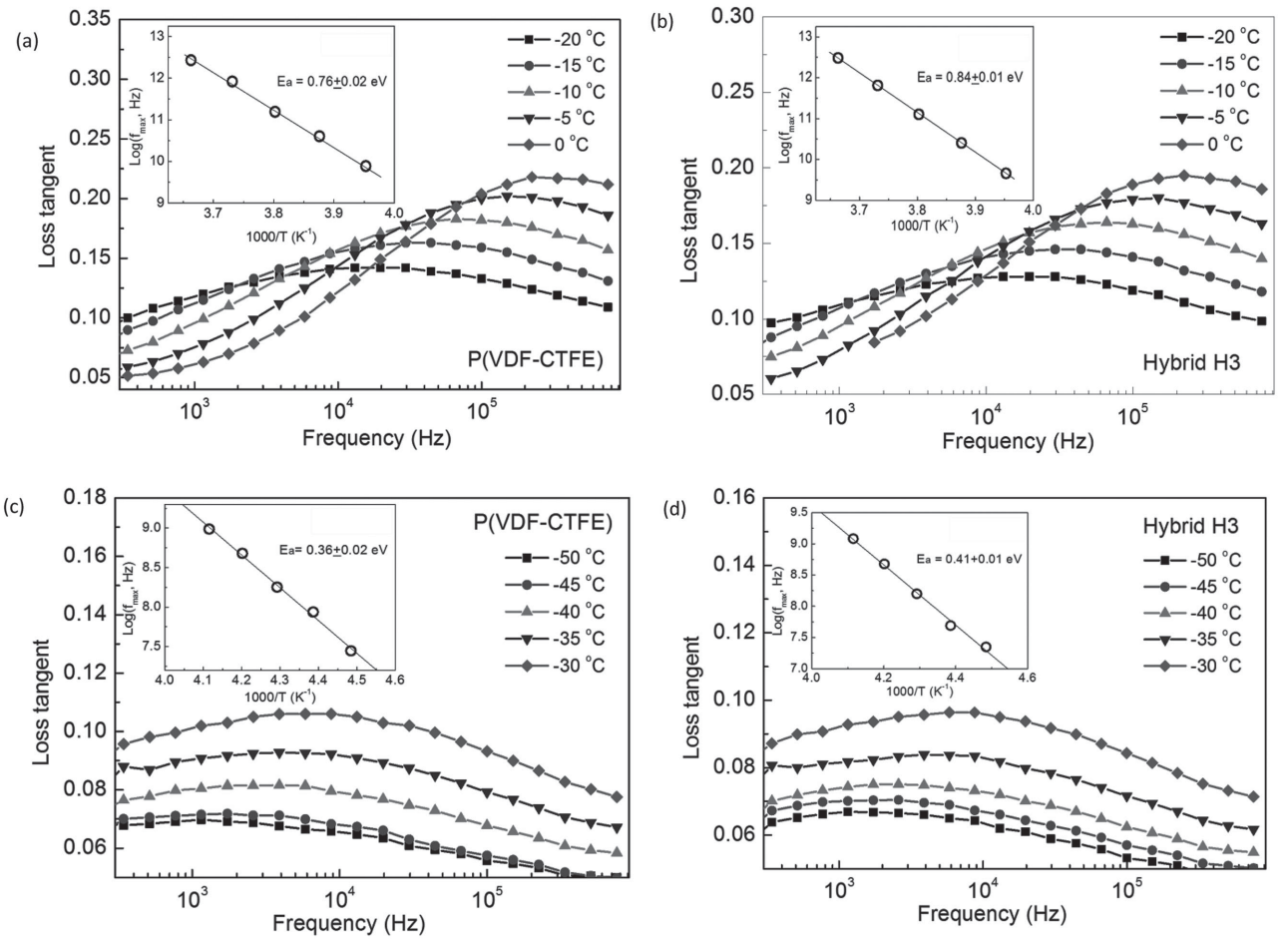

Figure 6. Dielectric loss versus frequency of the telechelic P(VDF-CTFE) at a) $T > T_g$ and c) $T < T_g$, and the hybrid **H3** at b) $T > T_g$ and d) $T < T_g$, focusing on the relaxation peak for selected temperatures as indicated on the plot. The insets are the corresponding Arrhenius plots.

force is generated from the oppositely charged electrodes, which subsequently creates the electromechanical compressive stress on polymer films. At the electrical breakdown field, the electromechanical stress exceeds yield stress of polymers, leading to collapse of the dielectric. A more quantitative assessment of the impact of the mechanical properties of polymer dielectric on dielectric strength has been performed according to the electromechanical breakdown model, $E_{eb} = (2\sigma_y/(\varepsilon_0\varepsilon))^{1/2}$, where E_{eb} is the electromechanical breakdown field, σ_y is the yield stress of the dielectric, ε_0 is the permittivity of free space, and ε is the relative permittivity of the dielectric.[44] The yield stresses of the hybrids and pristine P(VDF-CTFE) are determined from the intersection of the elastic and inelastic tangent lines from stress–strain curves (Supporting Information, Figure S7). As summarized in Table 3, E_{eb} matches closely the trend of mechanical properties as a function of the Ta-O content. Apparently, cross-linking network and incorporated Ta-O bonds strengthen the hybrids and provide higher resistance to the electromechanical breakdown.

Table 2. Activation energy derived from dielectric spectroscopy.

Sample	Activation energy [eV] $T > T_g$	Activation energy [eV] $T < T_g$
P(VDF-CTFE)	0.76 ± 0.02	0.36 ± 0.02
H1	0.81 ± 0.02	0.38 ± 0.01
H2	0.85 ± 0.02	0.40 ± 0.02
H3	0.84 ± 0.01	0.41 ± 0.01
H4	0.85 ± 0.01	0.42 ± 0.01
H5	0.86 ± 0.02	0.42 ± 0.02

2.5. Energy Storage Capability

The electric displacement–electric field (D–E) loops of the optimized hybrid **H3** and solution-processed pristine P(VDF-CTFE) were measured with a 10 Hz unipolar triangle signal (**Figure 10**), where the stored energy density is derived from the D–E loop by integration of the area between the charge curve and the ordinate, and the discharged energy density is determined by the area between the discharge curve and the ordinate. As plotted in **Figure 11**, the maximum released energy density of the solution-processed P(VDF-CTFE) is ~6.4 J cm^{-3} at 350 MV m^{-1}, consistent with the previous reports.[45] Notably, the hybrid **H3** discharges an U_e of ~18 J cm^{-3} at 500 MV m^{-1}, representing a 180% increase over the neat ferroelectric polymer and 15 times

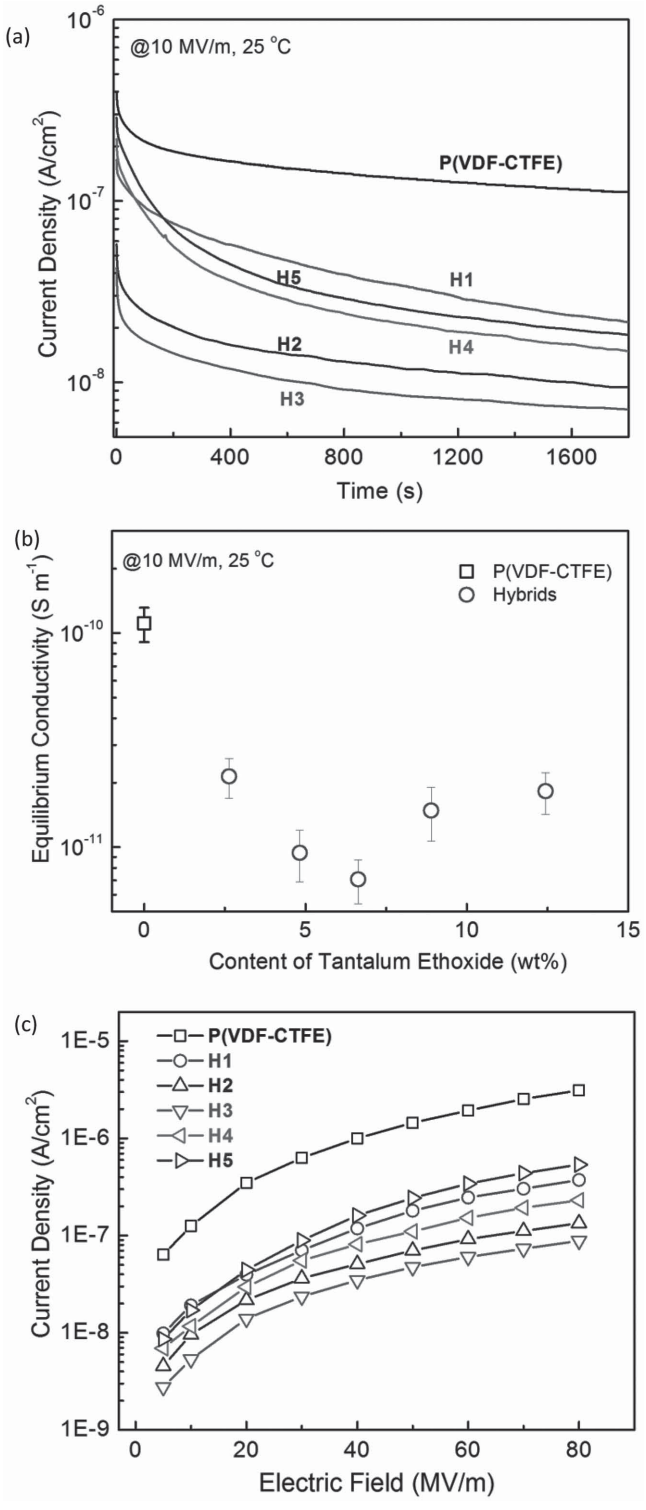

Figure 7. a) The evolution of DC current density under an electric field of 10 MV m^{-1} measured at 25 °C. b) The dependence of DC equilibrium conductivity on the compositions of the hybrids under an electric field of 10 MV m^{-1}. c) The dependence of DC current density on the applied electric field.

greater than that of biaxially oriented polypropylenes (BOPP), i.e., 1.2 J cm^{-3} at 640 MV m^{-1}, the polymer dielectric currently used in high energy density capacitors.[46]

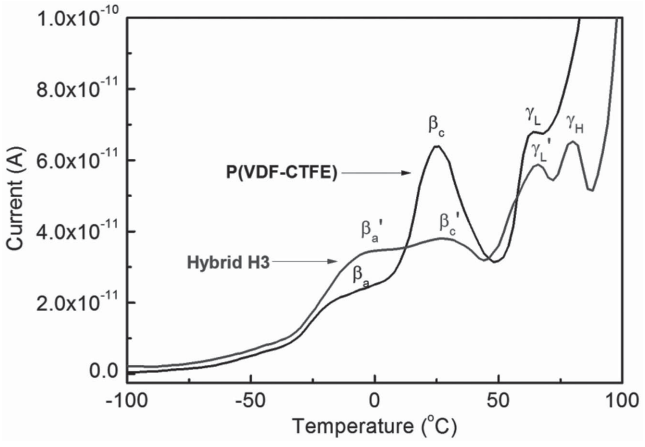

Figure 8. TSDC curves of the pristine P(VDF-CTFE) and the hybrid **H3**.

For ferroelectric materials, the energy loss at high fields consists of ferroelectric loss related to hysteresis and conduction loss stemming from electrical conduction.[47] In addition to a lower conductivity as shown in Figure 7b, the smallest crystalline size in **H3** as revealed in XRD is believed to benefit greatly the switchability of ferroelectric domains, resulting in reduced ferroelectric loss. Indeed, compared with the neat P(VDF-CTFE), the slimmer loops of **H3** stand for its lower energy loss (as indicated by the area enclosed in the loops) and smaller remnant polarization (i.e., the electric displacement at zero electric field) under the applied fields. As a direct result of lower loss and higher breakdown strength, **H3** is hence able to release more energy than the pristine P(VDF-CTFE).

3. Conclusions

In summary, we have demonstrated cross-linked Ta-O-P(VDF-CTFE) hybrids as a new class of solution-processed dielectric materials. It is found that the hybrids combining organic and inorganic constituents at the molecular level display reduced

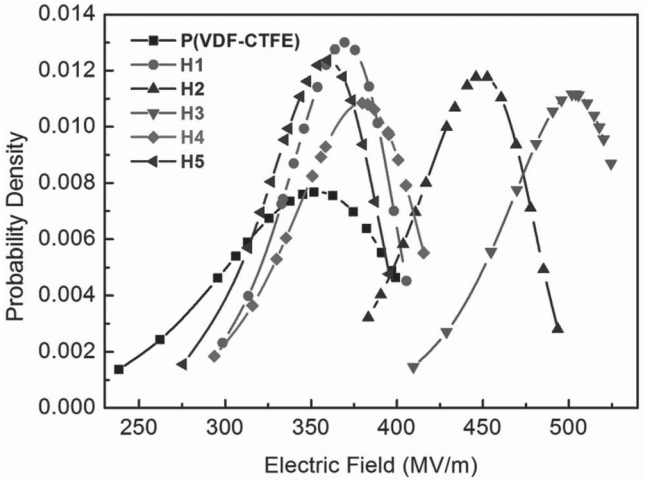

Figure 9. The Weibull distribution of breakdown fields of the P(VDF-CTFE) and the hybrids.

Table 3. Yield stress, calculated electromechanical breakdown strengths (E_{eb}), and Weibull breakdown strengths of the samples.

Sample	Yield stress [MPa]	Calculated E_{eb} [MV m^{-1}]	Experimental E_b [MV m^{-1}]	β
P(VDF-CTFE)	9.1	446	360	7.49
H1	10.1	475	372	13.11
H2	11.8	516	455	14.48
H3	13.6	554	505	15.29
H4	16.2	608	383	11.24
H5	17.1	631	363	12.32

electrical conduction because of the presence of deep traps as verified in the TSDC spectra. Moreover, the hybrids possess smaller crystallite sizes than the pristine polymer, which facilitates the dipole orientation and yields lower remnant polarization and reduced ferroelectric loss. The formation of the cross-linked network also effectively improves the mechanical properties of the hybrids. Synergistically, these contribute to lower energy loss, greatly improved breakdown strength, and higher discharged energy density of the hybrids when compared to the neat ferroelectric polymer. This work not only provides an entirely new dimension for the modulation of dielectric and capacitive properties of polymers but also exemplifies the promise of organic–inorganic hybrids to realize high electrical energy densities, given that a wide range of metal alkoxides are available for structural tailoring.

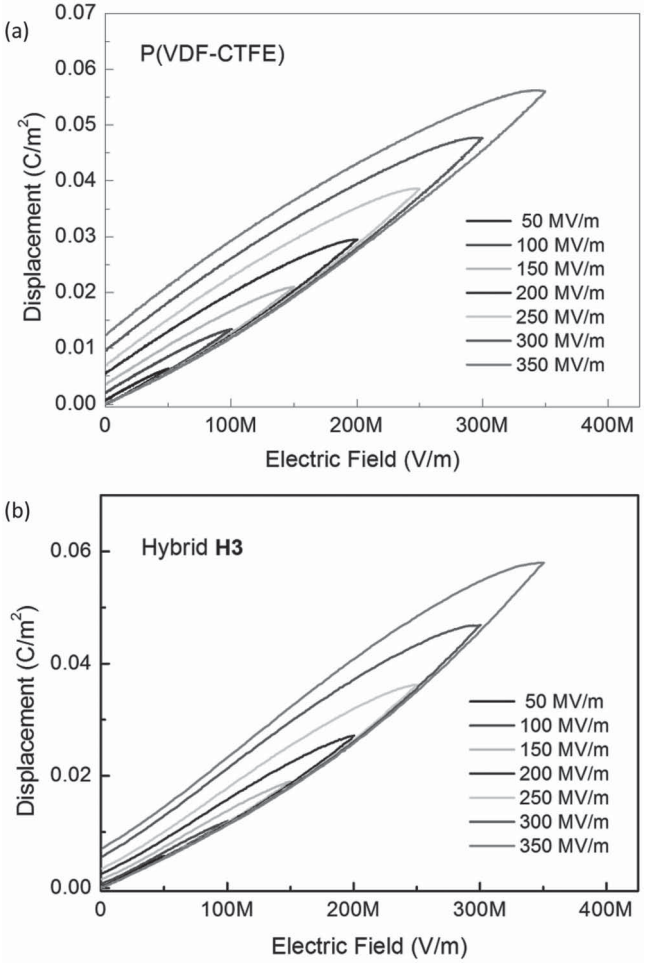

Figure 10. *D–E* loops of (a) solution-processed P(VDF-CTFE) and (b) the hybrid **H3**.

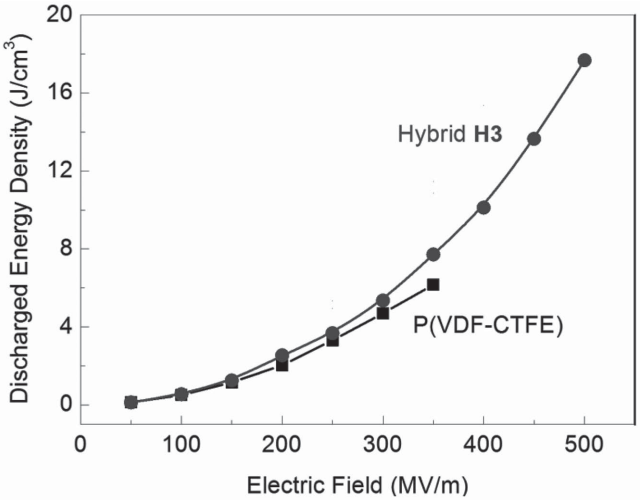

Figure 11. The stored and released energy density of solution-processed P(VDF-CTFE) and the hybrid **H3** as a function of electric field.

4. Experimental Section

Materials: All reagents were purchased from Aldrich and used without further purification unless otherwise noted. All the solvents used for the synthesis were HPLC grade. VDF and CTFE were purchased from SynQuest Laboratory Inc. and purified by the freeze–thaw process prior to use. All manipulations of gas-condense transfer were carried out with rigorous exclusion of oxygen and moisture on a dual-manifold Schlenk line with 10^{-6} Torr high vacuum. P(VDF-CTFE) (15 wt% of CTFE) was supplied by Solvay (Solef 31508). The functional initiator was prepared according to the literature procedure.[35]

Preparation of Telechelic P(VDF-CTFE)s: Initiated by 4-[(tetrahydropyran-2-yloxy) methyl] benzoic peroxide (300 mg), VDF (27 mL) and CTFE (2 mL) in anhydrous acetonitrile (30 mL) were polymerized in the Parr reactor under stirring at 90 °C. After 6 h, the reactor was cooled down, the residual gases were discharged and the solution was collected. The polymer was precipitated by the removal of the solvent, washed with the methanol three times, and dried in vacuum at 60 °C to yield 2.8 g white solid. To a mixture of tetrahydropyran ether terminated P(VDF-CTFE) (150 mg) in THF (100 mL) was added 3 M HCl (5 mL) and acetic acid (20 mL). The mixture was stirred at 60 °C for 3 h, and then was condensed in vacuo and poured into methanol (50 mL) to precipitate polymer. The polymer was collected by filtration, washed by methanol three times, and dried in vacuo at 60 °C.

Preparation of the Hybrids: The telechelic P(VDF-CTFE) was dissolved in anhydrous dimethylformamide (DMF) and mixed with tantalum ethoxide in anhydrous ethanol. Under stirring, the ethanol solution of tantalum ethoxide and 0.05 mL of distilled water was slowly added to the DMF solution of the chain-end functionalized polymer at room temperature. Stirred for 24 h, the mixture was cast on the octadecyltrichlorosilane (OTS) treated glass substrates and dried at 64 °C overnight. The prepared light brown film was then further dried in vacuo and heated to 150 °C stepwise at a rate of 10 °C h^{-1}. After heated at 150 °C for 72 h, the films were hot pressed at 200 °C under

1500 psi to remove the voids and residual solvent. The hybrid films with the tantalum ethoxide loadings of 5, 9, 13, 17, and 23 wt% were prepared with the thickness of 11–20 μm. P(VDF-CTFE) thin films with the thickness of 12 μm were hot pressed at 100 °C under 1500 psi after solution casting is prepared for the purpose of comparison.

Characterization: ^{1}H and ^{19}F NMR spectra were recorded on Bruker AM-300 spectrometer instrument at room temperature using tetramethylsilane (TMS) as an internal reference. Molecular weight and polydispersity of the synthesized polymer were determined in a THF mobile phase at a flow rate of 1.0 mL min^{-1} using a Viscotek Model 302 triple detection GPC system equipped with refractive index, right angle light scattering, and viscometer detectors. The thermal analysis data were obtained by a TA Instrument Q100 DSC at a heating and cooling rate of 10 °C min^{-1} and TA Q50 thermogravimetric analyzer at the heating rate of 10 °C min^{-1}. Crystal analysis was studied by the use of PANalytical xpert pro mpd theta-theta diffractometer. All data were analyzed using Jade software with a Gaussian–Lorentz superposition fitting functions. The cross-sectional morphology was explored using a JEOL 6700 field emission scanning electron microscope (FE-SEM). FTIR spectra were obtained in the attenuated total reflectance (ATR) mode using a diamond crystal as a contact to the samples on Bruker Vertex V70 spectrometer at room temperature. Dielectric constant and loss were acquired using an Agilent LCR meter (E4980A). Dielectric spectra were acquired over a broad frequency (10–10^6 Hz) and temperature (–100 to 100 °C) using a Hewlett Packard 4284A LCR meter in conjunction with a Delta Design oven model 2300. *D–E* loops were recorded using a modified Sawyer–Tower circuit. The dielectric breakdown field was determined by applying a linear ramp voltage at a rate of 500 V s^{-1} on the polymer film in accordance with the ASTM D149 standard. Resistivity and conductivity were obtained under a electric field provided by a Hewlett Packard 4140B pA meter/voltage source and KEPCO BOP 1000M amplifier in a Delta Design 2300 oven. TSDC was measured using Hewlett Packard 4140B pA meter with Kepco BOP 1000M as a high voltage source and performed in a Delta Design 2300 oven. Gold electrodes of 2.6 μm diameter and typical thickness of 60 nm were sputtered on both sides of the samples for the electrical measurements. Tensile tests were conducted at the pulling rate of 25 cm min^{-1} on the TA Instruments RSA-G2 Dynamic Mechanical Analyzer.

Supporting Information

Supporting Information is available from the Wiley Online Library or from the author.

Acknowledgements

K.H. and Q.L. contributed equally to this work. This work was supported by the US Office of Naval Research under Grant Number N00014-11-1-0342.

Received: March 18, 2015
Revised: April 6, 2015
Published online: May 4, 2015

[1] M. S. Whittingham, *MRS Bull.* **2008**, *33*, 411.
[2] E. Karden, S. Ploumen, B. Fricke, T. Miller, K. Snyder, *J. Power Sources* **2007**, *168*, 2.
[3] Y. Cao, P. C. Irwin, K. Younsi, *IEEE Trans. Dielectr. Electr. Insul.* **2004**, *11*, 797.
[4] S. Ducharme, *ACS Nano* **2009**, *3*, 2447.
[5] J. H. Pikul, H. G. Zhang, J. Cho, P. V. Braun, W. P. King, *Nat. Commun.* **2013**, *4*, 1732.
[6] Z. M. Dang, J. K. Yuan, S. H. Yao, R. J. Liao, *Adv. Mater.* **2013**, *25*, 6334.
[7] M. Rabuffi, G. Picci, *IEEE Trans. Plasma Sci.* **2002**, *30*, 1939.
[8] B. J. Chu, X. Zhou, K. L. Ren, B. Neese, M. R. Lin, Q. Wang, F. Bauer, Q. M. Zhang, *Science* **2006**, *313*, 334.
[9] Z. M. Dang, J. B. Wu, L. Z. Fan, C. W. Nan, *Chem. Phys. Lett.* **2003**, *376*, 389.
[10] G. Subodh, V. Deepu, P. Mohanan, M. T. Sebastian, *Appl. Phys. Lett.* **2009**, *95*, 062903.
[11] X. Zhou, X. H. Zhao, Z. G. Suo, C. Zou, J. Runt, S. Liu, S. H. Zhang, Q. M. Zhang, *Appl. Phys. Lett.* **2009**, *94*, 162901.
[12] N. Parvatikar, M. V. N. Ambika Prasad, *J. Appl. Polym. Sci.* **2006**, *100*, 1403.
[13] A. B. Afzal, M. J. Akhtar, M. Nadeem, M. M. Hassan, *J. Phys. Chem. C* **2009**, *113*, 17560.
[14] R. Schroeder, L. A. Majewski, M. Grell, *Adv. Mater.* **2005**, *17*, 1535.
[15] J. Li, P. Khanchaitit, K. Han, Q. Wang, *Chem. Mater.* **2010**, *22*, 5350.
[16] V. V. Ginzburg, K. Myers, S. Malowinski, R. Cieslinski, M. Elwell, M. Bernius, *Macromolecules* **2006**, *39*, 3901.
[17] N. Guo, S. A. DiBenedetto, P. Tewari, M. T. Lanagan, M. A. Ratner, T. J. Marks, *Chem. Mater.* **2010**, *22*, 1567.
[18] Q. Wang, L. Zhu, *J. Polym. Sci., Part B: Polym. Phys.* **2011**, *49*, 1421.
[19] J. K. Nelson, *Dielectric Polymer Nanocomposites*, Springer, New York **2010**.
[20] J. Y. Li, L. Zhang, S. Ducharme, *Appl. Phys. Lett.* **2007**, *90*, 132901.
[21] A. J. Lovinger, *Science* **1983**, *220*, 1115.
[22] Y. Lu, J. Claude, B. Neese, Q. M. Zhang, Q. Wang, *J. Am. Chem. Soc.* **2006**, *128*, 8120.
[23] L. Zhu, Q. Wang, *Macromolecules* **2012**, *45*, 2937.
[24] J. Claude, Y. Lu, K. Li, Q. Wang, *Chem. Mater.* **2008**, *20*, 2078.
[25] X. Zhou, B. J. Chu, B. Neese, M. R. Lin, Q. M. Zhang, *IEEE Trans. Dielectr. Electr. Insul.* **2007**, *14*, 1133.
[26] Q. Li, G. Z. Zhang, F. H. Liu, K. Han, M. R. Gadinski, C. X. Xiong, Q. Wang, *Energy Environ. Sci.* **2015**, *8*, 922.
[27] P. H. Hu, Y. Shen, Y. H. Guan, X. H. Zhang, Y. H. Lin, Q. M. Zhang, C. W. Nan, *Adv. Funct. Mater.* **2014**, *24*, 3172.
[28] X. Zhang, Y. Shen, Q. H. Zhang, L. Gu, Y. H. Hu, J. W. Du, Y. H. Lin, C. W. Nan, *Adv. Mater.* **2015**, *27*, 819.
[29] Q. Li, K. Han, M. R. Gadinski, G. Z. Zhang, Q. Wang, *Adv. Mater.* **2014**, *26*, 6244.
[30] G. Z. Zhang, Q. Li, H. M. Gu, S. L. Jiang, K. Han, M. R. Gadinski, M. A. Haque, Q. M. Zhang, Q. Wang, *Adv. Mater.* **2015**, *27*, 1450.
[31] V. Tomer, G. Polizos, C. A. Randall, E. Manias, *J. Appl. Phys.* **2011**, *109*, 074113.
[32] S. P. Fillery, H. Koerner, L. Drummy, E. Dunkerley, M. F. Durstock, D. F. Schmidt, R. A. Vaia, *ACS Appl. Mater. Interfaces* **2012**, *4*, 1388.
[33] C. Chaneliere, J. L. Autran, R. A. B. Devine, B. Balland, *Mater. Sci. Eng. R.* **1998**, *22*, 269.
[34] K. Kukli, M. Ritala, M. Leskela, *J. Electrochem. Soc.* **2001**, *148*, 35.
[35] K. Li, S. W. Liang, Y. Y. Lu, Q. Wang, *Macromolecules* **2007**, *40*, 4121.
[36] C. H. An, K. J. Sugimoto, *Electrochem. Soc.* **1992**, *139*, 1956.
[37] C. J. Huang, *Thin Solid Films* **2005**, *478*, 332.
[38] T. Ōishi, T. Nakazawa, A. Katou, *Electron. Comm. JPN-2* **1993**, *76*, 50.
[39] Y. Lu, J. Claude, L. E. Norena-Franco, Q. Wang, *J. Phys. Chem. B* **2008**, *112*, 10411.
[40] J. Li, S. I. Seok, B. J. Chu, F. Dogan, Q. M. Zhang, Q. Wang, *Adv. Mater.* **2009**, *21*, 217.
[41] A. Torres, J. Jiménez, B. Vega, J. A. De Saja, *J. Mater. Sci.* **1987**, *22*, 1623.
[42] Y. Takahashi, K. Miyaji, *Macromolecules* **1983**, *16*, 1789.
[43] M. Ieda, *IEEE Trans. Dielectr. Electr. Insul.* **1980**, *15*, 206.
[44] J. Claude, Y. Lu, Q. Wang, *Appl. Phys. Lett.* **2007**, *91*, 212904.
[45] Z. C. Zhang, Q. J. Meng, T. C. M. Chung, *Polymer* **2009**, *50*, 707.
[46] M. Rabuffi, G. Picci, *IEEE Trans. Plasma Sci.* **2002**, *5*, 1939.
[47] P. Khanchaitit, K. Han, M. R. Gadinski, Q. Li, Q. Wang, *Nat. Commun.* **2013**, *4*, 2845.